Available online at BCREC website: https://bcrec.id

Bulletin of Chemical Reaction Engineering & Catalysis, 17 (4) 2022, 699-711

Research Article

Synthesis of $NiFe_2O_4/SiO_2/NiO$ Magnetic and Application for the Photocatalytic Degradation of Methyl Orange Dye under UV Irradiation

Poedji Loekitowati Hariani[1,*], Muhammad Said[1], Addy Rachmat[1], S. Salni[2], Nabila Aprianti[3], Anisa Fitri Amatullah[1]

[1]*Research Group on Magnetic Materials, Department of Chemistry, Faculty of Mathematics and Natural Sciences, Universitas Sriwijaya, Ogan Ilir 30662, Indonesia*
[2]*Department of Biology, Faculty of Mathematics and Natural Sciences, Universitas Sriwijaya, Ogan Ilir 30662, Indonesia*
[3]*Doctoral Program of Environmental Science, Graduate School, Universitas Sriwijaya, Palembang 30139, Indonesia.*

Received: 6th September 2022; Revised: 30th September 2022; Accepted: 30th September 2022
Available online: 5th October 2022; Published regularly: December 2022

Abstract

$NiFe_2O_4/SiO_2/NiO$ magnetic was successfully synthesized using $NiFe_2O_4$, SiO_2, and NiO as the core, interlayer, and shell, respectively. $NiFe_2O_4/SiO_2/NiO$ under UV light irradiation was used for photocatalytic degradation of methyl orange dye with different pH, catalyst dose, and initial dye concentration. This composite was characterized by X-ray Diffraction (XRD), Fourier Transform Infra-Red (FTIR), Scanning Electron Microscopy-Electron Dispersive X-ray Spectroscopy (SEM-EDs), Vibrating Sample Magnetometer (VSM), UV-Vis Diffuse Reflectance Spectroscopy (UV-Vis DRS), and Point of Zero Charge (pHpzc). The results showed that the composite is a superparamagnetic material with a saturation magnetization value of 44.13 emu/g. It also has a band gap of 2.67 eV with a pHpzc of 6.33. The optimum conditions for photocatalytic degradation were at pH of 4; 0.50 g/L catalyst dose, and 10 mg/L initial concentration. $NiFe_2O_4/SiO_2/NiO$ degradation efficiency to methyl orange dye was 95.76%. The photocatalytic degradation in different concentrations follows the pseudo-first-order, where the greater the concentration, the smaller the constant rate (k). After five cycles of repeated usage, $NiFe_2O_4/SiO_2/NiO$ has good catalytic performance as well as efficient and favourable of a recyclable photocatalyst.

Keywords: $NiFe_2O_4/SiO_2/NiO$; magnetic; photocatalytic degradation; methyl orange dye

How to Cite: P.L. Hariani, M. Said, A. Rachmat, S. Salni, N. Aprianti, A.F. Amatullah, (2022). Synthesis of $NiFe_2O_4/SiO_2/NiO$ Magnetic and Application for the Photocatalytic Degradation of Methyl Orange Dye under UV Irradiation. *Bulletin of Chemical Reaction Engineering & Catalysis*, 17(4), 699-711 (doi: 10.9767/bcrec.17.4.15788.699-711)

Permalink/DOI: https://doi.org/10.9767/bcrec.17.4.15788.699-711

1. Introduction

Dye is an indispensable material in several industrial activities, such as textiles, food, cosmetics, pharmaceuticals, leather, paper, and soap [1,2]. Furthermore, synthetic dyes have a complex structure with toxic, carcinogenic, and mutagenic properties [3]. Dyes are easily soluble in water, difficult to degrade naturally, and has a long lifespan time in the environment. Dyes can also block the penetration of light into water, thereby inhibit the photosynthesis process

* Corresponding Author.
Email: puji_lukitowati@mipa.unsri.ac.id (P.L. Hariani)

and growth of aquatic organisms. The existence of dyes in the water interferes with aesthetics [4,5]. Methyl orange is often used in industries and as a pH indicator in laboratories. It has a molecular formula, namely $C_{14}H_{14}N_3SO_3Na$, with a molecular weight of 327.34 g/mol. Furthermore, it is classified as anionic with an azo group (N=N). The aromatic amine group in its chemical structure is carcinogenic due to the production of benzidine compounds through biotransformation [6]. A previous study revealed that more than 50% of the dyestuffs used in industry are azo dyes [7].

Various methods have been used to reduce dyes including ultra-filtration [8], electrochemical degradation [9], coagulation-flocculation [10], precipitation [11], ion exchange removal [12], adsorption [5], and photocatalytic degradation [13]. Among these methods, the advanced oxidation processes based on reactive oxygen species (ROS) has attracted researchers in recent years [14]. This method has advantages such as the ability to convert pollutants from wastewater into less hazardous compounds, the process occurs in a short time and at room temperature. Moreover, it does not produce secondary toxic products, where organic pollutants can be mineralized into simpler and less toxic materials, such as mineral acids, CO_2, and H_2O [15].

Semiconductors can absorb photons equal to or more than the gap energy, causing the formation of positive holes and electrons. The positive hole reacts with water molecules and produce hydroxyl radicals (•OH). Electrons in the conduction band are trapped by oxygen to produce superoxide radicals ($•O_2^-$). Furthermore, the interaction between hydroxyl, superoxide radicals, and dyes adsorbed on the semiconductor surface produces degradation products [16]. Several semiconductor materials can be used for photocatalytic degradation of dyes, such as TiO_2 [17], NiO [18], ZnO [19], CuO [20], and $BiVO_4$ [21]. Nickel oxide (NiO) is one of semiconductors, which is a *p*-type with a band gap range of 3.6–4.0 eV [22,23]. It has high conductivity, stability, and catalytic properties. The material has also been used for the photodegradation of methylene blue, malachite green [24], orange II [18], and methyl orange [25].

The disadvantages of Nickel oxide as a catalyst include low adsorption capacity and a wide band gap. Semiconductors with wide band gap show low photon absorbing efficiencies, such as TiO_2 with 5% [26] and ZnO with 10% [27]. Other drawbacks are the recombination of photo-induced e^-, the separation of the catalyst after the photocatalytic degradation process, and the occurrence of corrosion in an acid or alkaline environment during the photocatalytic degradation process [28]. Therefore, is it necessary to increase catalyst and catalytic activity [29]. The modification of catalyst with other compounds can increase the effectiveness of degradation, for example incorporated catalys with magnetic compounds, separation can be easily and quickly using permanent magnets without filtering from aqueous media. The ferrite materials have the general formula MFe_2O_4, where M is a divalent metal, such as Ni, Fe, Cd, Mg, Cu, Co, and Zn [30]. One of these is $NiFe_2O_4$, which has several advantages, including high electrical resistivity, chemical and mechanical stability, and excellent magnetic properties [31]. Modification of NiO with $NiFe_2O_4$ reduces the band gap of composite, where ferrite materials often have a band gap of ~2 [32].

To avoid the interaction between $NiFe_2O_4$ and NiO, another compound must be provided to serve as support [33]. SiO_2 can be used as a layer to prevent interaction. Another study reported that Fe_3O_4 coated with SiO_2 and TiO_2 as the outer thin layer could degrade methylene blue and ciprofloxacin dyes by 95% within 90 minutes [34]. SiO_2 can also protect ferrite compounds from agglomeration [35].

In this study, a core/interlayer/shell magnetic composite was synthesized, namely $NiFe_2O_4/SiO_2/NiO$. The product was characterized using XRD, FTIR, SEM-EDS, VSM, UV-Vis DRS, and pHpzc methods. The $NiFe_2O_4/SiO_2/NiO$ was used for photocatalytic degradation of methyl orange dye under UV radiation. Therefore, this study aims to determine the effect of pH of a solution, initial dye concentration, and irradiation time on photocatalytic degradation ability, kinetics, and catalysts reusability.

2. Materials and Methods

2.1 Materials

The chemicals used include $Ni(NO_3)_2.6H_2O$, $Fe(NO_3)_3.9H_2O$, NaOH, HCl, NH_4OH, methyl orange dye, tetraethyl orthosilicate (TEOS), ethanol from Merck, Germany, and distilled water.

2.2. Synthesis of $NiFe_2O_4$

The synthesis of $NiFe_2O_4$ was carried out using the coprecipitation method. A total of 6.58 g $Ni(NO_3)_2·6H_2O$ and 15.62 g $Fe(NO_3)_3·9H_2O$ were dissolved in 50 mL distilled water. The mixture was then stirred for

10 minutes and flowed with N_2 gas along with increasing temperature to 70 °C. NaOH 2 M solution was gradually added to obtain a pH of ± 11. The precipitate obtained, $NiFe_2O_4$, was washed using distilled water and ethanol until neutral pH was achieved. The solid powder separated from the solution using an external magnet and dried in an oven at 80 °C for 5 hours. Furthermore, it was calcined at 450 °C for 2 hours.

2.3. Synthesis of $NiFe_2O_4/SiO_2$

$NiFe_2O_4/SiO_2$ was synthesized using a modified Stober method. A total of 4 g of $NiFe_2O_4$ was placed in a 250 mL Erlenmeyer, followed by adding 10 mL ethanol. The ultrasonic process is carried out for 2 hours. Subsequently, 10.8 mL of 25% ammonia solution was added, and the following ultrasonic process was continued for 1 hour. A total of 20 mL TEOS solution was then added gradually and ultrasonicated for ± 60 minutes. The precipitate ($NiFe_2O_4/SiO_2$) was separated using centrifugation at 8000 rpm for 20 minutes, and was washed with distilled water and ethanol until it reached a neutral pH. It was then separated from the solution using an external magnet and dried in the oven at 80 °C for 5 hours, followed by calcination at 450 °C for 2 hours.

2.4. Synthesis of $NiFe_2O_4/SiO_2/NiO$

The synthesis of $NiFe_2O_4/SiO_2/NiO$ was carried out based on the modified method by Wang *et al.* [36]. A total of 1 g of $NiFe_2O_4/SiO_2$, 110 mL of distilled water, and ethanol (1:1) were placed in a blue-cap glass bottle and sonicated for 80 minutes. After adding 4 g urea, the sonification process was continued for 30 minutes. Subsequently, 120 mL of 0.1 M $Ni(NO_3)_2.6H_2O$ was added to the mixture, and sonification was carried out for 30 minutes. The precipitate ($NiFe_2O_4/SiO_2/NiO$), was separated from the solution using an external magnet and dried in an oven at 105 °C for 12 hours. The product was then washed with distilled water and separated using a centrifuge. It was dried in oven at 60 °C for 6 hours and calcined at 400 °C for 2 hours.

2.5. Catalyst Characterizations

$NiFe_2O_4$, $NiFe_2O_4/SiO_2$, and $NiFe_2O_4/SiO_2/NiO$ were analyzed using X-ray Diffraction (XRD PANalytical X'Pert PRO), with Cu-Kα radiation at λ = 0.15418 Å, 40 kV voltage, and range 2θ = 10-90°. Furthermore, morphology and elemental composition were analyzed using Scanning Electron Microscopy equipped with an energy dispersive spectrometer (SEM-EDS JSM 6510). Fourier Transform Infrared (FTIR, Prestige 21, Shimadzu) used to determine the functional groups in the wave number 400-4000 cm^{-1}. Meanwhile, the Vibration Sample Magnetometer (VSM Oxford Type 1.2 T) helps to assess the magnetic hysteresis loop. The absorbance and band gap was determined using UV-Vis Diffuse Reflectance Spectroscopy (UV-Vis DRS) analysis (Orion Aquamate 8000) at a wavelength of 200-800 nm. The dye concentration was evaluated using a UV-Vis spectrophotometer (Type Orion Aquamate 8000). Total organic carbon was evaluated with the Total Organic Carbon Analyzer (TOC Teledyne Tekmar).

2.6. Point of Zero Charges (pHpzc) Determination

The determination of pHpzc was based on a modified procedure of Behzadi *et al.* [37], where 0.1 g of $NiFe_2O_4/SiO_2/NiO$ was added to 25 mL of 0.1 M $NaNO_3$ solution. The pH value was adjusted to 2-12 using 0.1 M HNO_3 solution and 0.1 M NaOH. The mixture was then stirred with a shaker for 2 hours and left for 24 hours. Initial and final pH was determined using a pH meter. Subsequently, pHpzc was evaluated from a graph plot of the initial pH of the solution vs. ΔpH.

2.7. Photocatalytic Activity

Photocatalytic degradation experiments were performed using the batch method with UV radiation of 40 W. The variables used include effect of pH (2-8), dose (0.25; 0.5; 0.75 and 1.0 g/L) and initial dye concentration (10, 20, 30, and 40 mg/L). The experiment was carried out in a closed reactor at room temperature. A total of 50 mL methyl orange dye was placed in the reactor and stirred for 40 minutes to obtain adsorption-desorption equilibrium, followed by irradiation for 20, 40, 60, 80, 100, 120, and 140 minutes. The remaining dye after photocatalytic degradation was determined using a UV-Vis spectrophotometer. The ratio of the concentration for each time (*C)* with the initial concentration (C_0) was calculated using C/C_0, while the degradation efficiency was expressed by Equation (1):

$$Degradation\ Efficiency\ (\%) = \frac{C_0 - C}{C_0} x100\% \qquad (1)$$

2.8. Reusability of $NiFe_2O_4/SiO_2/NiO$

$NiFe_2O_4/SiO_2/NiO$ was applied for photocatalytic degradation of methyl orange dye un-

der optimum conditions. Subsequently, it was washed with distilled water and dried in an oven for 3 hours at 70 ºC. Calcination was then carried out at 300 ºC for ± 2 hours to remove organic substances [38]. $NiFe_2O_4/SiO_2/NiO$ was further reused for the process with a total of 5 repetitions.

3. Results and Discussion

3.1. Characterization of $NiFe_2O_4$, $NiFe_2O_4/SiO_2$, and $NiFe_2O_4/SiO_2/NiO$

The XRD spectra of $NiFe_2O_4$, $NiFe_2O_4/SiO_2$, and $NiFe_2O_4/SiO_2/NiO$ are presented in Figure 1. $NiFe_2O_4$ XRD spectra showed a peak at 2θ = 30.29°; 35,68°; 43.39°; 53.93°; 57.45°; 63.04°; and 79.61°. The 2θ angle was in line with JCPDS No. 54-0964 (standard card $NiFe_2O_4$), namely 30.1°; 35.3°; 43.0°; 53.7°; 56.5°; and 62.4° from the plane of 220, 311, 400, 422, 511, 440. Furthermore, the peak of $NiFe_2O_4/SiO_2$ appeared at the same angle, but decreased in intensity, namely 30.26°; 35.67°; 43,35°; 53.89°; 57.38°; and 63.23°. Coating with SiO_2 showed a new peak with low intensity and wide at 2θ of 23°, which is a characteristic of its amorphous nature [39]. The XRD characterization of $NiFe_2O_4/SiO_2/NiO$ showed the similar, namely 30.27°; 35.72°; 43. 38, 53.85°; 57.46°, and 63.21°. The addition of the peak was observed at an angle of 37.18° (111), and it also occurred in the spectra of NiO. Some of them also overlapped with those of $NiFe_2O_4$, such as 43.38° (200) and 63.21° (220). NiO also has the same peak, but it has a higher intensity than $NiFe_2O_4$ and $NiFe_2O_4/SiO_2$. The calculation results of the crystal size of $NiFe_2O_4$ using the Debye-Scherrer equation was 63.23 nm, while values of 53.56 nm and 48.53 nm were obtained for $NiFe_2O_4/SiO_2$ and $NiFe_2O_4/SiO_2/NiO$. The coating of $NiFe_2O_4$ with SiO_2 led to a decrease in crystal size because the material can prevent its agglomeration.

The FTIR spectra of $NiFe_2O_4$, $NiFe_2O_4/SiO_2$, and $NiFe_2O_4/SiO_2/NiO$ observed at wave numbers 400-4000 cm^{-1} are presented in Figure 2. The results showed that all materials have boad peak at wavenumbers 3400 cm^{-1} and 1600 cm^{-1}, indicating the presence of O–H groups from the water adsorbed by the catalyst [40]. The wave number of 400-700 cm^{-1} are characteristics of stretching vibration metal-oxides, such as Fe–O and Ni–O. Fe–O stretching vibrations from $NiFe_2O_4$ appeared at all peaks, namely 580.57 cm^{-1}, 590.65 cm^{-1}, and 588.23 cm^{-1}. Strong peak asymmetry of Si–O–Si occurred at wave numbers of 1085.12 cm^{-1} for $NiFe_2O_4/SiO_2$ and 1022.92 cm^{-1} for $NiFe_2O_4/SiO_2/NiO$. In $NiFe_2O_4/SiO_2$, the Si–O–H vibrational bond was observed at 958.12 cm^{-1} due to the interaction of SiO_2 with water molecules. This peak did not occur in $NiFe_2O_4/SiO_2/NiO$. Shi *et al.* [41] reported that a spinel structure of Ni^{2+}–O bond was observed in the area around 470 cm^{-1}, in this study it was observed at 453.30 at 453.30 cm^{-1} for $NiFe_2O_4/SiO_2$ and 459.69 cm^{-1} for $NiFe_2O_4/SiO_2/NiO$.

The morphological differences between $NiFe_2O_4$ and $NiFe_2O_4/SiO_2$ are presented in Figure 3. $NiFe_2O_4$ was heterogeneous and large in size, while the surface of $NiFe_2O_4/SiO_2$ shows the presence of coating particles. $NiFe_2O_4/SiO_2/NiO$ morphology was more homogeneous with almost the same particle size. Figure 4 shows the elemental mapping of $NiFe_2O_4/SiO_2/NiO$. Elements of Ni and O appear to spread on the catalyst's surface. This

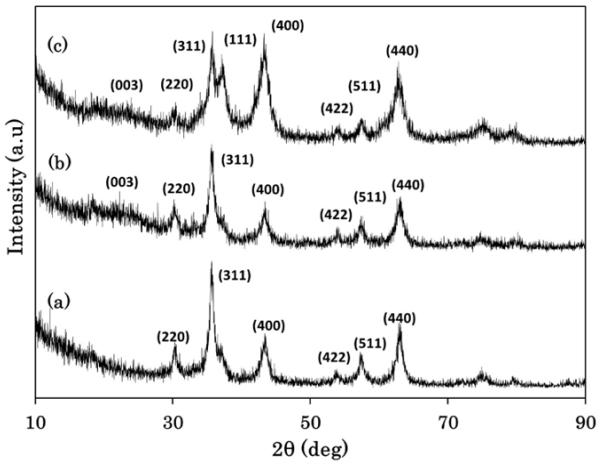

Figure 1. XRD pattern of (a) $NiFe_2O_4$, (b) $NiFe_2O_4/SiO_2$, and (c) $NiFe_2O_4/SiO_2/NiO$

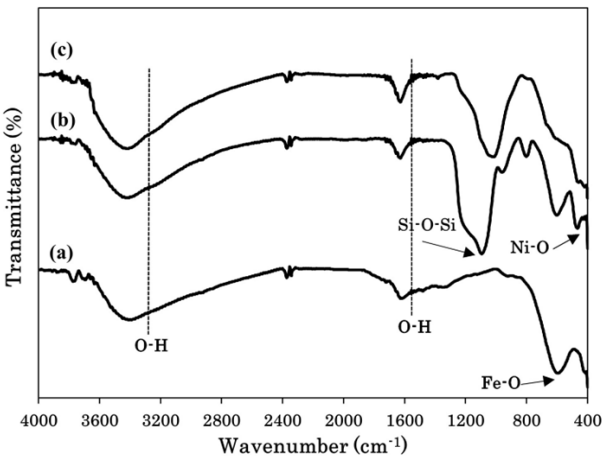

Figure 2. FTIR spectra of (a) $NiFe_2O_4$, (b) $NiFe_2O_4/SiO_2$, and (c) $NiFe_2O_4/SiO_2/NiO$

indicates that NiO has been distributed on the surface of $NiFe_2O_4/SiO_2$. Table 1 shows the analysis results of the constituent elements of $NiFe_2O_4$, $NiFe_2O_4/SiO_2$, and $NiFe_2O_4/SiO_2/NiO$ using EDS. $NiFe_2O_4$ is composed of elements, Ni, Fe, and O. The addition of Si indicates that SiO_2 has successfully coated $NiFe_2O_4$. The increase in the percentage of Ni in $NiFe_2O_4/SiO_2/NiO$ shows indicates the addition of Ni from NiO.

The magnetic properties of $NiFe_2O_4$, $NiFe_2O_4/SiO_2$, and $NiFe_2O_4/SiO_2/NiO$ are presented in Figure 5. $NiFe_2O_4$ has a saturation magnetization value of 50.37 emu/g, which was greater than the value obtained after synthesis using solution combustion of 47.32 emu/g [42]. The bulk saturation value was 56 emu/g [43]. The saturation magnetization of $NiFe_2O_4$ was greater than $NiFe_2O_4/SiO_2$ and

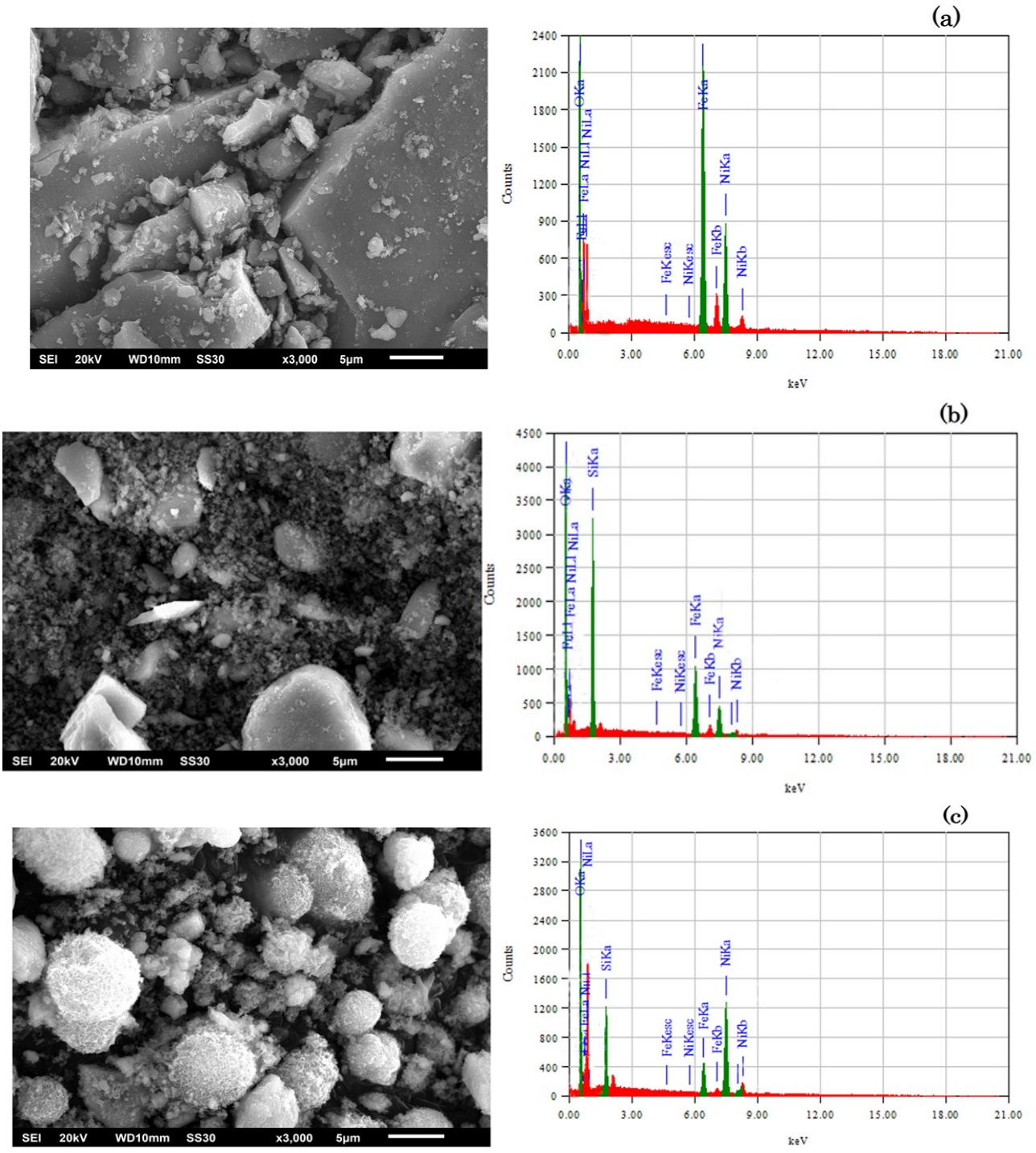

Figure 3. Morphology and EDS spectra of (a) $NiFe_2O_4$, (b) $NiFe_2O_4/SiO_2$, and (c) $NiFe_2O_4/SiO_2/NiO$

$NiFe_2O_4/SiO_2/NiO$ by 46.37 emu/g and 44.13 emu/g, respectively. The magnetic properties decreased due to $NiFe_2O_4$ coating with non-magnetic SiO_2, which isolated $NiFe_2O_4$ from the magnetic field. Another study reported that the saturation magnetization value decreased as follows: $CoFe_2O_4$ > $CoFe_2O_4/SiO_2$ > $CoFe_2O_4/SiO_2/TiO_2$ [44]. Magnetic properties are influenced by crystal size. The larger the crystal size, the greater the saturation magnetization [45]. In this study, the largest crystal size was obtained from $NiFe_2O_4$.

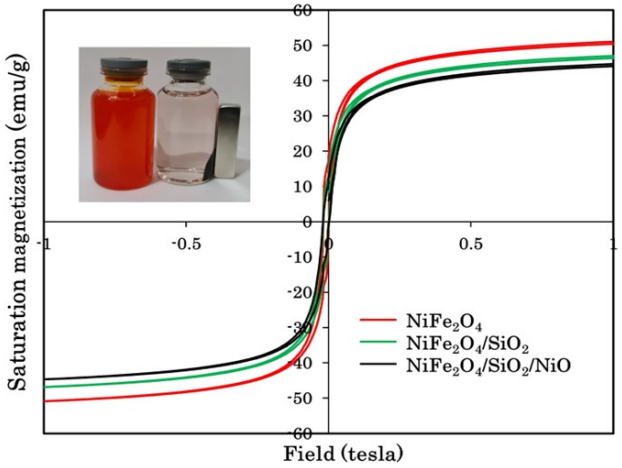

Figure 5. Magnetic properties of $NiFe_2O_4$, $NiFe_2O_4/SiO_2$, and $NiFe_2O_4/SiO_2/NiO$

The amount of energy absorbed by the catalyst depends on the optical band gap energy, namely the difference between the valence and conduction bands. The decrease in the gap (E_g) by the doping process prevents electron-hole pair recombination (e^-/h^+) and increases photocatalytic activity [46]. The optical E_g was determined using the following equation [41]:

$$ahv = A(hv - E_g)^n \quad (2)$$

where, a is the absorption coefficient, h is Planck's constant, and n is the light frequency. The value of n was ½ for direct semiconductors, while a value of 2 was obtained for indirect variants. NiO is a catalyst that is classified as a direct semiconductor. A in the Equation (2) is the proportionality constant, and E_g is the optical band gap.

The analysis of optical properties using UV-Vis DRS is shown in Figure 6. The wavelength obtained in this study from 200-800 nm. Band gap value is obtained from the curve of $(ahv)^2$ vs hv (photon energy). The $NiFe_2O_4$ band gap was 1.81 eV, which was lower than $NiFe_2O_4/SiO_2$ and $NiFe_2O_4/SiO_2/NiO$ by 2.21 eV and 2.67 eV, respectively. Another study reported that semiconductor doping using ferrite compounds reduced the band gap. For example, the band gap for ZnO decreased by 3.12 eV to 1.71 eV after doping by $NiFe_2O_4$ [46].

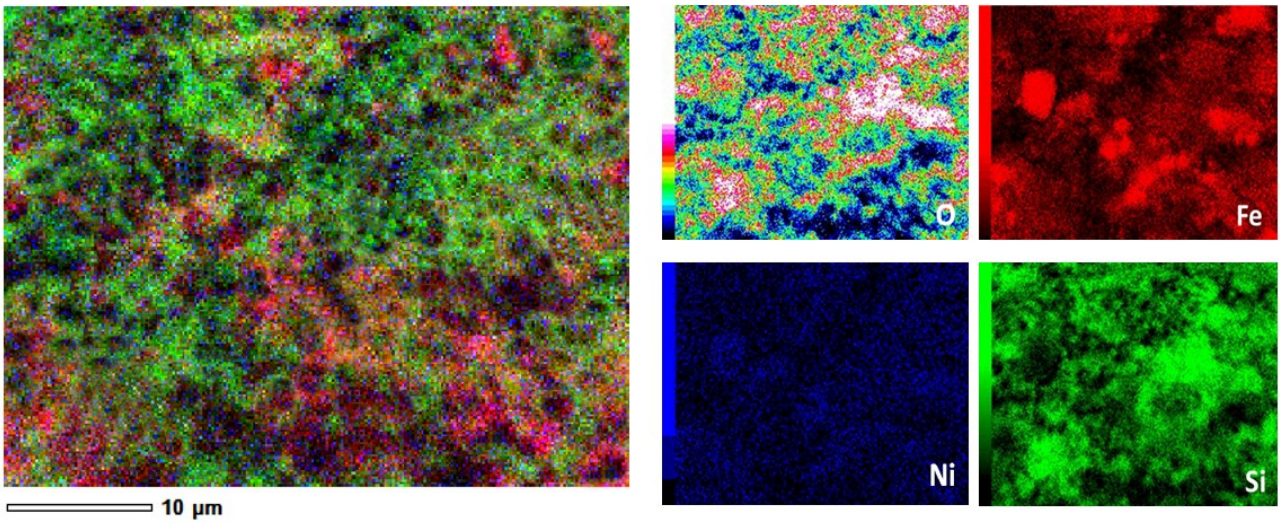

Figure 4. Elemental mapping of $NiFe_2O_4/SiO_2/NiO$

Table 1. Elemental composition of $NiFe_2O_4$, $NiFe_2O_4/SiO_2$, and $NiFe_2O_4/SiO_2/NiO$

Materials	Ni (%)	Fe(%)	O(%)	Si(%)
$NiFe_2O_4$	24.99	46.63	27.36	-
$NiFe_2O_4/SiO_2$	12.88	23.30	48.23	13.96
$NiFe_2O_4/SiO_2/NiO$	30.83	16.70	41.47	10.25

3.2. Photocatalytic Degradation of Methyl Orange Dye

Photocatalytic degradation using $NiFe_2O_4/SiO_2/NiO$ on methyl orange dye carried out through the batch method by analyzing the effect of pH, catalyst dose, and dye concentration on dye removal with an irradiation time of 0-140 minutes (interval 20 minutes). Figure 7a shows a graph of the initial pH Versus ΔpH plot to obtain pHpzc with a value of 6.33. The material surface has a negative and positive charge when pHpzc < pH and pHpzc > pH, respectively [47]. Figure 7b shows the effect of pH on the amount of degraded methyl orange dye, which had a 50 mL volume and 20 mg/L concentration of metyl orange dye. The methyl orange dye had a pH in a range of 3.1-4.5 [48]. At pH < pHpzc, $NiFe_2O_4/SiO_2/NiO$ is positively charged, while methyl orange dye is anionic (negatively charged), causing an attraction between them.

A control was carried out without irradiation for 40 minutes to create adsorption-desorption equilibrium, and the C/C_0 curve shows a sloping trend. Meanwhile, it decreased sharply with irradiation, indicating rapid degradation. The same phenomenon occurred in the photocatalytic degradation of rhodamine B

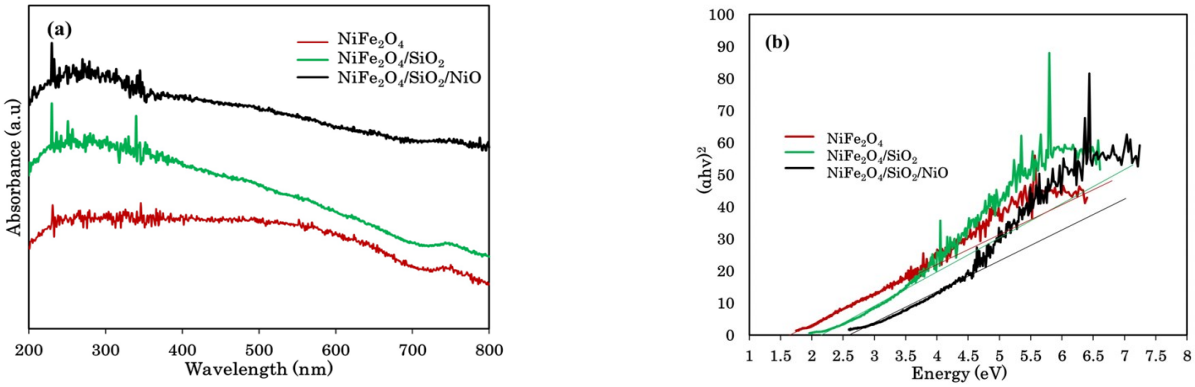

Figure 6. Spectra of (a) UV-Vis DRS and (b) Band gap energies of $NiFe_2O_4$, $NiFe_2O_4/SiO_2$, and $NiFe_2O_4/SiO_2/NiO$

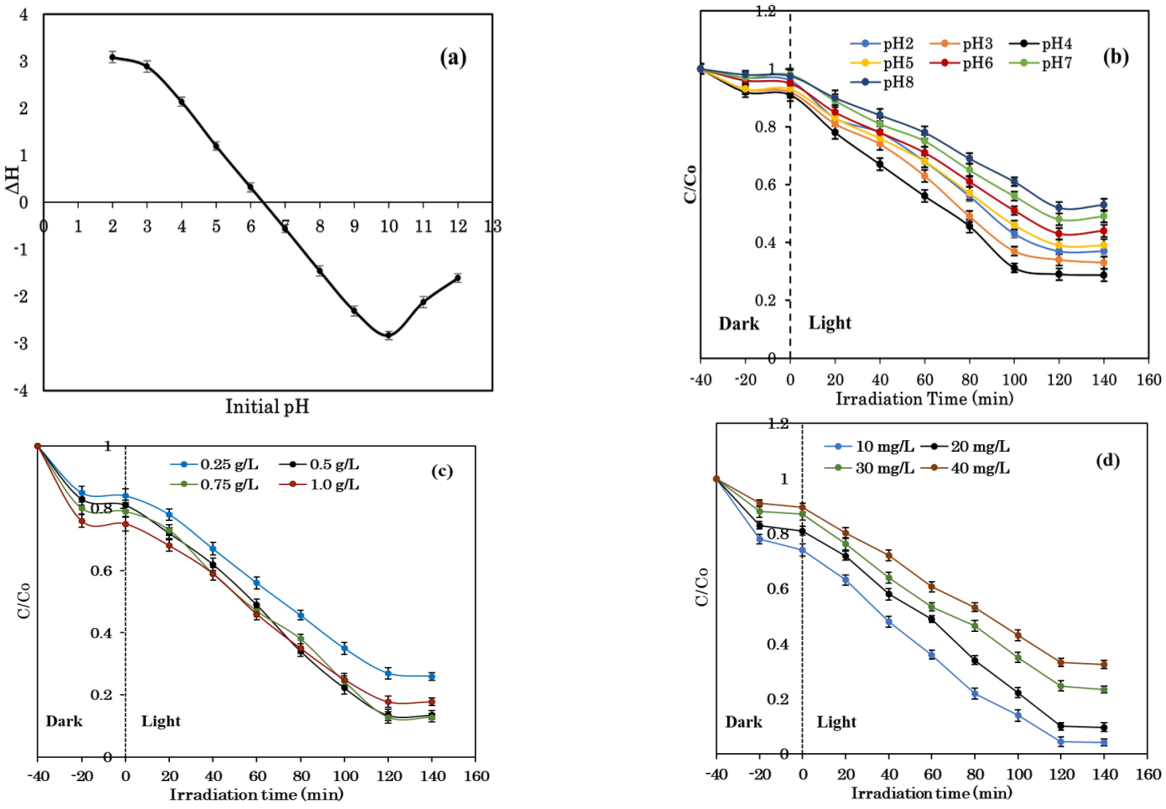

Figure 7. (a) pHpzc $NiFe_2O_4/SiO_2/NiO$, and photocatalytic degradation curve of methyl orange dye as a function of (b) pH, (c) Initial concentration, and (d) $NiFe_2O_4/SiO_2/NiO$ doses

dye using γ-Fe_2O_3@SiO_2@TiO_2. The addition of catalyst for one hour without irradiation showed that the degradation percentage was less than 10% [49]. In this study, the highest degradation efficiency was at pH of 4. The higher the pH, the more the hydroxide ions (OH^-), which causes competition between the dye and hydroxide ions. Another study reported that the highest degradation efficiency for methyl orange dye occurred at a pH of 4 using $CoFe_2O_4/SiO_2/TiO_2$ [35].

The effect of catalyst dose on the photocatalytic degradation of methyl orange was analyzed using different catalyst concentrations from 0.25 to 1.0 g/L. The results obtained are presented in Figure 7c. At 0-40 minutes, the percentage of dye degradation increased drastically from a dose of 0.25 to 1.0 g/L. However, there was no increase after 120 minutes. The higher the catalyst dose, the more active sites (hydroxyl free radicals) are available, which leads to more degradation. The solution becomes cloudy and opaque when excess catalyst is added, reducing light transmission to the dye [48]. Alkaykh *et al*. [50] reported that at high doses of catalyst, molecular activation was inhibited due to collisions between catalysts, which reduced the reaction rate. The optimum dose obtained was 0.5 g/L with a degradation efficiency of 86.56%.

Figure 7d shows that the greater the concentration of the dye, the smaller the degraded substance. Furthermore, the higher the concentration, the more it can interact with the active surface of the catalyst, but this condition prevents the penetration of light [35]. The smallest value of C/C_0 was obtained from 10 mg/L of methyl orange with degradation efficiency of 95.76%. In this study, UV light was used as an irradiation source with a constant intensity. The effectiveness of photocatalytic degradation can be increased by optimizing the use of energy consumption, which is the most suitable intensity for the photocatalytic degradation process [51]. Table 2 shows the comparison of several photocatalyst for the methyl orange dye degradation, where $NiFe_2O_4/SiO_2/NiO$ had a better degradation efficiency than others.

The photocatalytic degradation mechanism of the dye methyl orange dye (MO) is described as follows [54]:

$$NiFe_2O_4/SiO_2/NiO + h\nu \rightarrow NiFe_2O_4/SiO_2/NiO\ (e_{CB}^- + h_{VB}^+) \quad (3)$$

$$e_{CB}^- + O_2 \rightarrow \cdot O_2^- \quad (4)$$

$$h_{VB}^+ + H_2O \rightarrow \cdot OH + H^+ \quad (5)$$

$$\cdot O_2^- + H^+ \rightarrow \cdot OH_2 \quad (6)$$

$$\cdot O_2^- + H_2O \rightarrow \cdot HO_2 + OH^- \quad (7)$$

$$\cdot OH_2 + H_2O \rightarrow H_2O_2 + \cdot OH \quad (8)$$

$$H_2O_2 \rightarrow 2 \cdot OH \quad (9)$$

$$MO\text{-}NiFe_2O_4/SiO_2/NiO + \cdot OH/\cdot O_2^- \rightarrow NiFe_2O_4/SiO_2/NiO + CO_2 + H_2O + \text{other product} \quad (10)$$

The first reaction is the adsorption of MO on the surface of the catalyst. Conduction band electrons (e_{CB}^-) and valence bond holes (h_{VB}^+) are photogenerated when $NiFe_2O_4/SiO_2/NiO$ is exposed to UV irradiation which is greater than the band gap energy. The adsorbed hydroxyl ions and oxygen on the catalyst with the MO form hydrogen bonds. MO on the catalyst surface will be attacked by $\cdot OH$ and $\cdot O_2^-$, resulting in decolorization [46,54].

Total organic carbon analysis can determine the mineralization level of dyes obtained from photocatalytic degradation. The level was not fully achieved, but it indicates the occurrence of the mineralization process [55]. For example, the TOC removal for phenol using $CoFe_2O_4/SiO_2/TiO_2$ in 120 minutes was 87%, and the TOC removal of paraquat after 180 minutes using N-doped TiO_2@SiO_2@Fe_3O_4 was 84.71% [35,55]. In this study, the initial and after-degradation TOC values were determined under optimum conditions: pH of 4, 0.5 g/L photocatalyst dose, methyl orange dye concentration of 10 mg/L, and irradiation time of 120 minutes. The TOC removal value obtained was 87.60%. These results indicated that the dye

Table 2. Comparison of several photocatalysts for the methyl orange dye degradation

Catalyst	pH	Dosis (g/L)	Concentration (mg/L)	Time (min)	Efficiency (%)	Reff.
NiO	2	2.0	10	30	90	24
$Fe_3O_4/SiO_2/TiO_2$	-	0.25	30	300	90.2	39
MnO_2/CeO_2	2.6	1.0	10	60	90	52
Chitosan-Zn-Mg	3	0.15	10	120	74.05	4
TiO_2	3	-	15	240	93	53
$NiFe_2O_4/SiO_2/NiO$	4	0.50	10	120	95.76	In this work

had been decomposed into minerals, such as H_2O and CO_2, and the remnants have been converted into other organic materials.

3.3. Photocatalytic Degradation Kinetics

Photocatalytic degradation can be illustrated using pseudo-first-order [56], and the equation is as follows:

$$\ln C_0/C_t = kt \quad (3)$$

where, C_0 and C_t are the initial concentration and concentration of dye at the time (mg/L), k is the rate constant (min^{-1}), and t is the irradiation time (min). The initial concentration of the dye has a fundamental effect on the degradation rate, where the kinetic rate constant decreases as the concentration increases [57]. Figure 8 shows a pseudo-first-order graph with varying methyl orange dye levels of 10, 20, 30, and 40 mg/L. The correlation coefficient (R^2) value indicates the suitability of photocatalytic degradation, which was close to 1. Furthermore, the k values obtained were 0.0212, 0.0157, 0.0112 and 0.0083 min^{-1}. Li *et al.* [56] reported that the degradation rate of semiconductors was predicted to follow the Langmuir–Hinshelwood type of kinetics and first-order decomposition, assuming the degradation occurs directly on the surface of the catalyst. Another study reported that the kinetics constants obtained for methyl orange dye using TiO_2 decreased as the concentration increased (0.015, 0.025, and 0.035 g/L), namely 0.00278 > 0.0023 > 0.00173 min^{-1} [53].

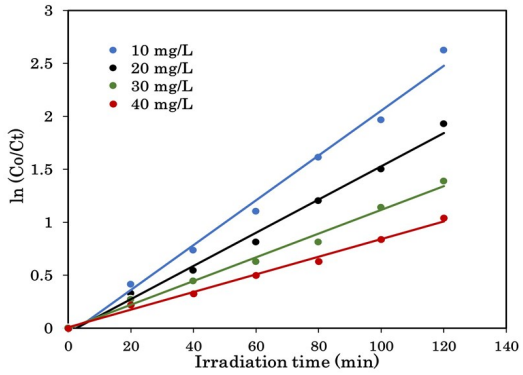

Figure 8. The photocatalytic degradation kinetics of $NiFe_2O_4/SiO_2/NiO$ in different methyl orange dye concentrations

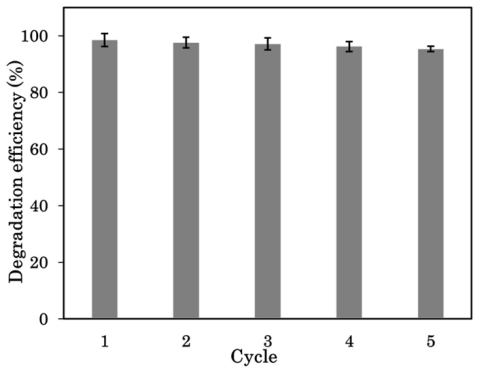

Figure 9. Reusability of $NiFe_2O_4/SiO_2/NiO$ for photocatalytic degradation of methyl orange dye

3.4. Photocatalyst Reusability

Evaluation of the stability and ability of $NiFe_2O_4/SiO_2/NiO$ used is presented in Figure 9. After its usage in the photocatalytic degradation process, it was separated from the solution using a permanent magnet. This catalyst was cleaned with deionization water and then calcined. Subsequently, it was reused for photocatalytic degradation of methyl orange dye. Five cycles showed a change in its ability from 98.51 to 95.36%. These results showed the adequate performance of $NiFe_2O_4/SiO_2/NiO$ as a photocatalyst.

The FTIR spectra of $NiFe_2O_4/SiO_2/NiO$ before and after being used as a catalyst showed similar spectra as shown in Figure 10. This indicates that the catalyst has high stability under UV light irradiation. The functional groups of the catalyst before and after use were the same, although there was a slight change in intensity.

4. Conclusion

In this study, a core/interlayer/shell magnetic composite was successfully synthesized, namely $NiFe_2O_4/SiO_2/NiO$, with a saturation magnetization value of 44.13 emu/g and a band gap of 2.67 eV. The EDS results confirmed that the product consisted of Ni, Fe, O, and Si, which indicated that the synthesis was suc-

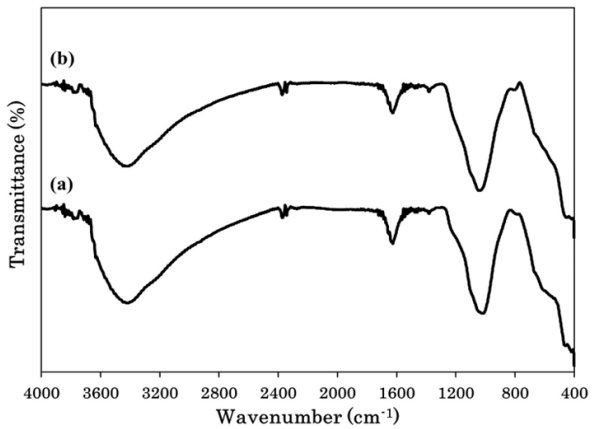

Figure 10. FTIR spectra of $NiFe_2O_4/SiO_2/NiO$ (a) before and (b) after reused five cycles for photocatalytic degradation

cessful. Photocatalytic degradation of methyl orange dye by $NiFe_2O_4/SiO_2/NiO$ under UV irradiation at pH 4, 0.5 g/L dose od catalyst, and 10 mg/L concentration of methyl orange dye for 120 minutes irradiation, has a degradation efficiency of 95.76%. The indicated that the mineralization of methyl orange dye by the effectiveness of the TOC was 87.60%. Experimental data showed that the photocatalytic degradation kinetics according a pseudo-first-order. $NiFe_2O_4/SiO_2/NiO$ has high stability and catalytic activity it was used in five cycles. Along with its low cost, high photocatalytic activity, stability, and easy separation by external magnet, the $NiFe_2O_4/SiO_2/NiO$ has broad prospects in large-scale wastewater treatment.

Acknowledgement

Author would thank to the Ministry of Education, Culture, Research and Technology for funded research of *Penelitian Dasar Unggulan Perguruan Tinggi* (PDUPT) scheme in 2022, under the contract No. 0063.01/UN9.3.1/PL/2022.

References

[1] Gusmao, K.A.G., Gurgel, L.V.A., Melo, T.M.S., Gil, L.F. (2013). Adsorption Studies of Methylene Blue and Gentian Violet on Sugarcane Bagasse Modified with EDTA Dianhydride (EDTAD) in Aqueous Solutions: Kinetic and Equilibrium Aspects. *Journal of Environmental Management*, 118, 135-143. DOI: 10.1016/j.jenvman.2013.01.017

[2] Ali, N., Said, A., Ali, F., Razig, F., Ali, Z., Bilal, M, Reinert, L., Iqbal, H.M.N. (2020). Photocatalytic Degradation of Congo Red Dye from Aqueous Environment Using Cobalt Ferrite Nanostructures: Development, Characterization, and Photocatalytic Performance. *Water, Air, & Soil Pollution*, 231(50), 1-16. DOI: 10.1007/s11270-020-4410-8

[3] Iwuozor, K., Ighalo, J.O, Emenike, E.C., Ogunfowora, L.A., Igwegbe, C.A. (2021). Adsorption of Methyl Orange: A Review on Adsorbent Performance. *Current Research in Green and Sustainable Chemistry*, 4, 1-6. DOI: 10.1016/j.crgsc.2021.100179

[4] Makeswari, M., Saraswathi, P. (2020). Photocatalytic Degradation of Methylene Blue and Methyl Orange from Aqueous Solution using Solar Light onto Chitosan Bi-metal Oxide Composite. *SN Applied Science*, 2(336), 1-12. DOI:10.1007/s42452-020-1980-4

[5] Alghamdi, A.A., Al-Odayni, A., Saeed, W.S., Almutairi, M.S., Alharthi, F.A., Aouak, T., Al-Kahtani, A. (2019). Adsorption of Azo Dye Methyl Orange from Aqueous Solutions Using Alkali-Activated Polypyrrole-Based Graphene Oxide. *Molecules*, 24, 1-17. DOI: 10.3390/molecules24203685

[6] Chen, D., Chen, J., Luan, X., Ji, H., Xia, Z. (2011). Characterization of Anion–Cationic Surfactants Modified Montmorillonite and Its Application for the Removal of Methyl Orange. *Chemical Engineering Journal*, 171, 1150-1158. DOI: 10.1016/j.cej.2011.05.013

[7] Ajmal, A., Majeed, I., Malik, R.N., Idriss H., Nadeem, M.A. (2014). Principles and Mechanisms of Photocatalytic Dye Degradation on TiO_2 Based Photocatalysts: a Comparative Overview. *RSC Advances*, 4, 37003-37026. DOI: 10.1039/C4RA06658H

[8] Fradj, A.B., Boubakri, A., Hafiane, A., Hamouda, S.B. (2020). Removal of Azoic Dyes from Aqueous Solutions by Chitosan Enhanced Ultrafiltration. *Results in Chemistry*, 2, 1-9. DOI: 10.1016/j.rechem.2019.100017

[9] Li, S., Zhao, Y., Chu, J., Li, W., Yu, H., Liu, G. (2013). Electrochemical Degradation of Methyl Orange on Pt–Bi/C Nanostructured Electrode by a Square-wave Potential Method. *Electrochimica Acta*, 92, 93-101. DOI: 10.1016/j.electacta.2013.01.012

[10] Igwegbe, C.A., Onukkwuli, O.D., Ighalo, J.O., Umembamalu, C.J. (2021), Electrocoagulation-flocculation of Aquaculture Effluent using Hybrid Iron and Aluminium Electrodes: A comparative Study. *Chemical Engineering Journal Advances*, 6,1-14. DOI: 10.1016/j.ceja.2021.100107

[11] Ali, M., Sarkar, A., Pandey, M.D., Pandey, S. (2006). Efficient Precipitation of Dyes from Dilute Aqueous Solutions of Ionic Liquids. *Analytical Sciences*, 22, 1051-1053. DOI: 10.2116/analsci.22.1051

[12] Huang, R., Zhang, Q., Yao, H., Lu, Z., Zhou, Q., Yan, D. (2021). Ion-Exchange Resins for Efficient Removal of Colorants in Bis(hydroxyethyl) Terephthalate. *ACS Omega*, 6(18), 12351-12360. DOI: 10.1021/acsomega.1c01477

[13] Hanif, M.K.H.M., Sapawe, N. (2020). A Short Review on Photocatalytic toward Dye Degradation. *Materials Today*, 31(1), A42-A47. DOI: 10.1016/j.matpr.2020.10.967

[14] Hassani, A., Krishnan, S., Scaria J., Eghbali, P., Nidheesh, P.V. (2021). Z-scheme Photocatalysts for Visible-light-driven Pollutants Degradation: A Review on Recent Advancements. *Current Opinion in Solid State and Materials Science*, 25(5), 1-25. DOI: 10.1016/j.cossms.2021.100941

[15] Solomon, R.V., Lydia, I.S., Merlin, J.P., Venuvanalingam, P. (2012). Enhanced Photocatalytic Degradation of Azo Dyes using Nano Fe_3O_4. *Journal of the Iranian Chemical Society*, 9, 101-109. DOI: 10.1007/s13738-011-0033-8

[16] Kitture, R., Koppikar, S.J., Kaul-Ghanekar, R., Kale, S.N. (2011). Catalyst Efficiency, Photostability and Reusability Study of ZnO Nanoparticles in Visible Light for Dye Degradation. *Journal of Physics and Chemistry of Solids*, 27(1), 60-66. DOI: 10.1016/j.jpcs.2010.10.090

[17] Lee, S.Y., Kang, D., Jeong, S., Do, H.T., Kim, J.H. (2020). Photocatalytic Degradation of Rhodamine B Dye by TiO_2 and Gold Nanoparticles Supported on a Floating Porous Polydimethylsiloxane Sponge under Ultraviolet and Visible Light Irradiation. *ACS Omega*, 5(8), 4233-4241. 10.1021/acsomega.9b04127

[18] Khan, N.A., Saeed, K., Khan, I., Gul, T., Sadiq, M., Uddin, A., Zakker I. (2022). Efficient Photodegradation of Orange II Dye by Nickel Oxide Nanoparticles and Nanoclay Supported Nickel Oxide Nanocomposite. *Applied Water Science*, 12(131), 1-10. DOI: 10.1007/s13201-022-01647-x

[19] Isai, K.A., Shrivastava, V.S. (2019). Photocatalytic Degradation of Methylene Blue using ZnO and 2%Fe–ZnO Semiconductor Nanomaterials Synthesized by Sol–Gel Method: a Comparative Study. *SN Applied Sciences*, 1(1247), 1-11. DOI: 10.1007/s42452-019-1279-5

[20] Nazim, M., Khan, A.A.P., Asiri, A.M., Kim, J.H. (2021). Exploring Rapid Photocatalytic Degradation of Organic Pollutants with Porous CuO Nanosheets: Synthesis, Dye Removal, and Kinetic Studies at Room Temperature. *ACS Omega*, 6, 2601-2612. DOI: 10.1021/acsomega.0c04747

[21] Hunge, Y.M., Uchida, A., Tominaga, Y., Fujii, Y., Ydav, A.A., Kang, S., Suzuki, N., Shitanda, I., Kondo, T., Itagaki, M., Yuasa, M., Gosavi, S., Fujishima, A., Terashima, C. (2021). Visible Light-Assisted Photocatalysis Using Spherical-Shaped $BiVO_4$ Photocatalyst. *Catalysts*, 11(4), 1-11. DOI: 10.3390/catal11040460

[22] Bordbar, M., Negahdar, N., Nasrollahzadeh, M. (2018). *Melissa Officinalis* L. Leaf Extract Assisted Green Synthesis of CuO/ZnO Nanocomposite for the Reduction of 4-nitrophenol and Rhodamine B. *Separation and Purification Technology*, 191, 295-300. DOI: 10.1016/j.jphotobiol.2018.03.016.

[23] Kganyago, P., Mahlaule-Glory, L.M., Mathipa, M.M., Ntsendwana, B., Mketo, N., Mbita, Z., Hintsho-Mbita N.C. (2018). Synthesis of NiO Nanoparticles via a Green Route using *Monsonia burkeana*: The Physical and Biological Properties. *Journal of Photochemistry and Photobiology B: Biology*, 182, 18-26. DOI: 10.1016/j.jphotobiol.2018.03.016

[24] Motene, K., Mahlaule-Glory, L.M., Ngoepe, N.M., Mathipa, M.M., HintshoMbita, N.C. (2021). Photocatalytic Degradation of Dyes and Removal of Bacteria using Biosynthesised Flowerlike NiO Nanoparticles. *International Journal of Environmental Analytical Chemistry*, 2021, 1-17. DOI: 10.1080/03067319.2020.1869730

[25] Barzinjy, A.A., Hamad, S.M. Aydin, S., Ahmed, M.H., Hussain, F.H.S. (2020). Green and Eco-friendly Synthesis of Nickel Oxide Nanoparticles and Its Photocatalytic Activity for Methyl Orange Degradation. *Journal of Materials Science: Materials in Electronics*, 31, 11303–11316. DOI: 10.1007/s10854-020-03679-y

[26] Moosavi, S., Li, R.Y.M., Lai, C.W., Yusof, Y., Gan, S., Akbarzadeh, O., Chowhurry, Z.Z., Yue, X., Johan, M.R. (2020). Methylene Blue Dye Photocatalytic Degradation over Synthesised Fe_3O_4/AC/TiO_2 Nano-Catalyst: Degradation and Reusability Studies. *Nanomaterials*, 10(12), 1-15. DOI: 10.3390/nano10122360

[27] Rahimi, S.M., Panahi, A.H., Moghadam, N. S. M., Allahyari, E., Nasseh, N. (2022). Breaking Down of Low-biodegradation Acid Red 206 Dye using Bentonite/Fe_3O_4/ZnO Magnetic Nanocomposite as a Novel Photo-catalyst in Presence of UV light. *Chemical Physics Letters*, 794, 1-11. DOI: 10.1016/j.cplett.2022.139480

[28] Hassani, A., Faraji, M., Eghbali, P. (2020). Facile Fabrication of mpg-C_3N_4/Ag/ZnO Nanowires/Zn Photocatalyst Plates for Photodegradation of Dye Pollutant. *Journal of Photochemistry and Photobiology A: Chemistry*, 400, 1-15. DOI: 10.1016/j.jphotochem.2020.112665

[29] Madihi-Bidgoli, S., Asanezhad, S., Yaghoot-Nezhad, A., Hassani, A. (2021). Azurobine Degradation using Fe_2O_3@multi-walled Carbon Nanotube Activated Peroxymonosulfate (PMS) under UVA-LED Irradiation: Performance, Mechanism and Environmental Application. *Journal of Environmental Chemical Engineering*, 9(6), 2-11. DOI: 10.1016/j.jece.2021.106660

[30] Hirthna, Sendhilnathan, S., Rajan, P.I., Adinaveen, T. (2018). Synthesis and Characterization of $NiFe_2O_4$ Nanoparticles for the Enhancement of Direct Sunlight Photocatalytic Degradation of Methyl Orange. *Journal of Superconductivity and Novel Magnetism*, 31, 1-9. DOI: 10.1007/s10948-018-4601-3

[31] Ishino, K., Narumiya, Y. (1988). Development of Magnetic Ferrites: Control and Application of Loss. *Ceramic Bulletin*, 66, 1469-1475. DOI:10.1002/CHIN.198820306

[32] Casbeer, E., Sharma, V.K., Li, X.Z. (2012). Synthesis and Photocatalytic Activity of Ferrites under Visible Light: A Review. *Separation and Purification Technology,* 87, 1-14. DOI: 10.1016/j.seppur.2011.11.034.

[33] Shan, A.Y., Ghazi, T.I.M., Rashid, S.A. (2010). Immobilisation of Titanium Dioxide onto Supporting Materials in Heterogeneous Photocatalysis: a Review. *Applied Catalysis A: General*, 389 (1), 1-8. DOI: 10.1016/j.apcata.2010.08.053

[34] Teixera, S., Mora, H., Blasse L., Martins, P.M., Carabineiro, S.A.C., Lanceros-Mendez, S., Kuhn, K., Cuniberti, G. (2017). Photocatalytic Degradation of Recalcitrant Micropollutants by Reusable $Fe_3O_4/SiO_2/TiO_2$ Particles. *Journal of Photochemistry and Photobiology A: Chemistry*, 345, 27-35. DOI: 10.1016/j.jphotochem.2017.05.024

[35] Hariani P.L., Said M., Salni, Aprianti N. and Naibaho Y.A.L.R. (2022). High Efficient Photocatalytic Degradation of Methyl Orange Dye in an Aqueous Solution by $CoFe_2O_4$-SiO_2-TiO_2 Magnetic Catalyst. *Journal of Ecological Engineering*, 23, 118-128. DOI: 10.12911/22998993/143908

[36] Wang, L., Huang, Y., Sun, X., Huang, H., Liu, P., Zong, M., Wang, Y. (2014). Synthesis and Microwave Absorption Enhancement of Graphene@Fe_3O_4@SiO_2@NiO Nanosheet Hierarchical Structures. *Nanoscale*, 6, 3157-3164. DOI: 10.1039/C3NR05313J

[37] Behzadi, S, Nonahal, B., Royaee, S.J., Asadi, A.A. (2020). $TiO_2/SiO_2/Fe_3O_4$ Magnetic Nanoparticles Synthesis and Application in Methyl Orange UV Photocatalytic Removal. *Water Science Technology*, 82 (11), 2432-2445. DOI: 10.2166/wst.2020.509

[38] Prasad, K.S., Shamshuddin, S.Z.M. (2022). Highly Efficient Conversion of Glycerol and t-Butanol to Biofuel Additives over AlPO Solid Acid Catalyst under Microwave Irradiation Technique: Kinetic Study. *Comptes Rendus Chimie*, 25, 149-170. DOI: 10.5802/crchim.132

[39] Chen, F., Yan, F., Chen, Q., Wang, Y., Han, L. (2014). Fabrication of Fe_3O_4@SiO_2@TiO_2 Nanoparticles Supported by Graphene Oxide Sheets for the Repeated Adsorption and Photocatalytic Degradation of Rhodamine B under UV Irradiation. *Dalton Transaction*, 43, 13537-13544. DOI: 10.1039/C4DT01702A

[40] Alzahrani, E. (2017). Photodegradation of Binary Azo Dyes Using Core-Shell $Fe_3O_4/SiO_2/TiO_2$ Nanospheres. *American Journal of Analytical Chemistry*, 8, 95-115. DOI: 10.4236/ajac.2017.81008

[41] Shi, M., Qiu, T., Tang, B., Zhang, G., Yao, R., Xu, W., Chen, J., Fu, X., Ning, H., Peng, J. (2021). Temperature-Controlled Crystal Size of Wide Band Gap Nickel Oxide and Its Application in Electrochomism. *Micromachines,* 12(80), 1-11. DOI: 10.3390/mi12010080.

[42] Hariani P.L., Said M., Rachmat A., Riyanti F., Pratiwi H.C. Rizki W.T. (2021), Preparation of $NiFe_2O_4$ Nanoparticles by Solution Combustion Method as Photocatalyst of Congo red. *Bulletin of Chemical Reaction Engineering & Catalysis*, 16, 481-490. DOI: 10.9767/bcrec.16.3.10848.481-490

[43] Tan, J., Zhang, W., Xia, A. (2013). Facile Synthesis of Inverse Spinel $NiFe_2O_4$ Nanocrystals and Their Superparamagnetic Properties. *Materials Research*, 16, 237-241. DOI: 10.1590/S1516-143920120050000157.

[44] Zielińska-Jurek A., Bielan Z., Dudziak S., Wolak I., Sobczak Z., Klimczuk T., Nowaczyk G., Hupka J. (2017). Design and Application of Magnetic Photocatalysts for Water Treatment. The Effect of Particle Charge on Surface FUnctionality. *Catalysts*, 7(360), 1-19. DOI: 10.3390/catal7120360

[45] Das, H., Inukai, A., Debnath, N., Kawaguchi, T., Sakamoto, N., Hoque, S.M., Aono, H., Shinazaki, K., Suzuki, H., Wakiya, N. (2018). Influence of Crystallite on the Magnetic and Heat Generation Properties of $La0.77Sr0.23MnO_3$ Nanoparticles for Hyperthermia Applications. *Journal of Physics and Chemistry of Solids*, 112, 179-184. DOI: 10.1016/j.jpcs.2017.09.030.

[46] Adeleke, J.T., Theivasanthi, T., Thiruppathi, M., Swaminathan, M., Akomolafe, T., Alabi, A.B. (2018). Photocatalytic Degradation of Methylene Blue by $ZnO/NiFe_2O_4$ Nanoparticles. *Applied Surface Science*, 455, 195-200. DOI: 10.1016/j.apsusc.2018.05.184

[47] Wu, L., Liu, X., Lv, G., Zhu, R., Tian, L., Liu, M., Li, Y., Rao, W., Liu, T. Liao L. (2021). Study on the Adsorption Properties of Methyl Orange by Natural One-dimensional Nano-mineral Materials with Diferent Structures. *Scientific Report*, 11, 1-11. DOI: 10.1038/s41598-021-90235-1

[48] Niu, P. (2013). Photocatalytic Degradation of Methyl Orange in Aqueous TiO_2 Suspensions. *Asian Journal of Chemistry*, 25(2), 1103-1106. DOI: 10.14233/ajchem.2013.13539

[49] Wang, F., Li, M., Yu, L., Sun, F., Wang, Z., Zhang, L., Zeng, H., Xu, X. (2017). Corn-like, Recoverable γ-Fe_2O_3@SiO_2@TiO_2 Photocatalyst Induced by Magnetic Dipole Interactions. *Scientific Reports*, 7, 1-10. DOI: 10.1038/s41598-017-07417-z

[50] Alkaykh, S., Mbarek, A., Ali-Shattle, E.E. (2020). Photocatalytic Degradation of Methylene Blue Dye in Aqueous Solution by $MnTiO_3$ Nanoparticles under Sunlight Irradiation. *Heliyon*, 6, 1-6. DOI: 10.1016/j.heliyon.2020.e03663

[51] Modirshahla, N., Behnajady, M.A., Rahbarfam, R., Hassani, A. (2012). Effects of Operational Parameters on Decolorization of C. I. Acid Red 88 by UV/H_2O_2 Process: Evaluation of Electrical Energy Consumption. *Clean – Soil, Air, Water*, 40(3), 298-302. DOI: 10.1002/clen.201000574

[52] Zhao, H., Zhang, G., Chong, S., Zhang, N., Liu, Y. (2015). MnO_2/CeO_2 for Catalytic Ultrasonic Decolorization of Methyl Orange: Process parameters and mechanisms. *Ultrosonic Sonochemistry*, 27, 474-479. DOI: 10.1016/j.ultsonch.2015.06.009

[53] Trablesi, H., Atheba, G.P., Hentati, O., Mariette, Y.D., Robert, D., Drogui, P., Ksibi, M. (2016). Solar Photocatalytic Decolorization and Degradation of Methyl Orange Using Supported TiO_2. *Journal of Advanced Oxidation Technologies*, 19(1), 79-84. DOI: 10.1515/jaots-2016-0110

[54] Ammar, S.H., Elaibi, A.I., Mohamme, I.S. (2020). Core/shell Fe_3O_4@Al_2O_3-PMo Magnetic Nanocatalyst for Photocatalytic Degradation of Organic Pollutants in an Internal Loop Airlift Reactor. *Journal of Water Process Engineering*, 37, 1-11. DOI: 10.1016/j.jwpe.2020.101240

[55] Pourzad, A., Sobhi, H.R., Behbahani, M., Esrafili, A., Kalantary, R.R., Kermani, M. (2020). Efficient Visible Light-induced Photocatalytic Removal of Paraquat using N-doped TiO_2@SiO_2@Fe_3O_4 Nanocomposite. *Journal of Molecular Liquids*, 299, 1-7. DOI: 10.1016/j.molliq.2019.112167

[56] Li, Y., Li, X., Li, J., Yin, J. (2006). Photocatalytic Degradation of Methyl Orange by TiO_2-coated Activated Carbon and Kinetic Study. *Water Research*, 40, 1119-1126. DOI: 10.1016/j.watres.2005.12.042

[57] Silva, da, C.G., Faria, J.L., (2003). Photochemical and Photocataytic Degradation of an Azo Dye in Aqueous Solution by UV Irradiation. *Journal of Photochemistry and Photobiology A: Chemistry*, 155, 133-143. DOI: 10.1016/S1010-6030(02)00374-X